Published in final edited form as:
J Biomech. 2014 March 3; 47(4): 834–846. doi:10.1016/j.jbiomech.2014.01.012.

Image-based modeling for better understanding and assessment of atherosclerotic plaque progression and vulnerability: Data, modeling, validation, uncertainty and predictions

Dalin Tang[a,b,*], **Roger D. Kamm**[c], **Chun Yang**[b,d], **Jie Zheng**[e], **Gador Canton**[f], **Richard Bach**[g], **Xueying Huang**[h], **Thomas S. Hatsukami**[i], **Jian Zhu**[j], **Genshan Ma**[j], **Akiko Maehara**[k], **Gary S. Mintz**[k], and **Chun Yuan**[l]

Dalin Tang: dtang@wpi.edu

[a]School of Biological Sciences and Medical Engineering, Southeast University, Nanjing, China

[b]Worcester Polytechnic Institute, Worcester, MA 01609, USA

[c]Massachusetts Institute of Technology, Cambridge, MA 02139, USA

[d]China Information Tech. Designing & Consulting Institute Co., Ltd., Beijing 100048, China

[e]Mallinkcrodt Inst. of Radiology, Washington University, St. Louis, MO 63110, USA

[f]Department of Mechanical Engineering, University of Washington, Seattle, WA 98195, USA

[g]Cardiovascular Division, Washington University, St. Louis, MO 63110, USA

[h]School of Mathematical Sciences, Xiamen University, Xiamen, Fujian 361005, China

[i]Division of Vascular Surgery, University of Washington, Seattle, WA, 98195, USA

[j]Department of Cardiology, Zhongda Hospital, Southeast University, Nanjing 210009, China

[k]The Cardiovascular Research Foundation, NY, NY, USA

[l]Deparment of Radiology, University of Washington, Seattle, WA 98195, USA

Abstract

Medical imaging and image-based modeling have made considerable progress in recent years in identifying atherosclerotic plaque morphological and mechanical risk factors which may be used in developing improved patient screening strategies. However, a clear understanding is needed about what we have achieved and what is really needed to translate research to actual clinical practices and bring benefits to public health. Lack of in vivo data and clinical events to serve as gold standard to validate model predictions is a severe limitation. While this perspective paper provides a review of the key steps and findings of our group in image-based models for human carotid and coronary plaques and a limited review of related work by other groups, we also focus

*Correspondence to: School of Biological Sciences and Medical Engineering, Southeast University, Nanjing, China / Worcester Polytechnic Institute, 100 Institute Road, Worcester, MA 01609, USA.

Conflict of interest statement: There is no conflict of interest with any other individuals or government in the paper.

on grand challenges and uncertainties facing the researchers in the field to develop more accurate and predictive patient screening tools.

Keywords

Atherosclerosis; Fluid-structure interaction; IVUS-based modeling; MRI-based modeling; Vulnerable plaques

1. Introduction and background

Atherosclerotic plaque initiation, progression and the final rupture are complex processes which involve many factors including mechanical forces (plaque stress, flow shear stress, blood pressure), plaque morphology (thin cap, lipid-rich necrotic core, calcification, hemorrhage, ulcer, etc.), cell activities (inflammation, remodeling), blood conditions (cholesterol level, injury-initiated blood changes), exercise, emotional stress, and genomic activities. The mechanisms causing plaque rupture and subsequent clinical events are not fully understood (Fuster, 1998; Fuster et al., 1990; Naghavi et al., 2003a, 2003b). Considerable progress has been made in recent years in medical imaging (Yuan et al., 2001a, 2001b; Underhill, et al., 2010), histopathological analysis (Stary et al., 1992, 1994, 1995; Virmani et al., 2000, 2006), biomechanical plaque material properties (Finet et al., 2004; Le Floc'h et al., 2012; Baldewsing et al., 2008), mechanical stress risk factors (Richardson et al., 1989; Arroyo and Lee, 1999; Ohayon et al., 2011; Loree et al., 1992). and computational models (Tang, 2006; Friedman et al., 2010) for better understanding of plaque progression, rupture and to develop possible better patient screening and plaque assessment schemes. Richardson's paper (2002) provided an excellent review for plaque biomechanical analysis, covering essential topics including plaque components, tissue, cap pathology, modeling, and rupture process. Fleg et al. (2012) gave an authoritative review of findings from several large clinical studies for detection of high-risk atherosclerotic plaques, available techniques, findings from patient follow-up studies, and future recommendations (Fleg et al., 2012). As recommended in the report, the grand challenge here is to find more sensitive and predictive risk factors, develop new patient screening tools, identify patients who are more vulnerable to plaque rupture and associated clinical events such as stroke and heart attack, and recommend proper treatment plans to prevent those events from happening.

Currently, plaque stenosis severity is still the primary factor used as guidance for treatment decisions in practice. However, closer examination of the results of recent clinical trials indicates current risk prediction is imprecise and the value of a particular intervention for each individual is uncertain. For example, among six major clinical trials assessing the efficacy of carotid endarterectomy (CEA) for prevention of stroke among patients with atherosclerotic carotid artery disease, results indicated that the number of patients needed to treat with CEA to prevent 1 stroke within 2 years varied from 8 to 83 (Gorelick, 1990), and the percentage in absolute risk of stroke at 2 years for patients treated medically vs. those undergoing CEA ranged from 1.2% to 12.9% (Gorelick, 1990; Barnett et al., 1999), with a median percentage at about 5%. This implies that most CEAs (> 90%) were performed among patients who were considered at risk but who, even without the surgery, would not have gone on to have a stroke and were therefore recommended because available screening

methods could not provide more accurate assessment and risk prediction. More accurate predictive screening methods are needed so that future plaque rupture can be predicted early and proper treatment can be recommended to prevent actual drastic clinical events and reduce the number of unnecessary surgeries.

Compared with the stenosis-based screening schemes, improvements are possible in the following areas: (a) use of medical images that can more accurately quantify plaque morphology, components, lumen dimensions, plaque surface characteristics, and plaque inflammation; (b) use of image-based modeling to establish the association of mechanical risk factors (plaque stress/strain, flow shear stress) with biological/clinical events; (c) use of patient follow-up and actual clinical data to identify risk factors with predictive power, quantify their prediction accuracy, and develop predictive methods for plaque rupture and related clinical events.

While it is generally agreed that mechanical forces play an important role in plaque progression and rupture, it has not yet been established that stress-based risk indicators could better predict plaque progression, rupture and drastic cardiovascular events (Wu et al., 2011). It is a paradigm change: most investigations based on available one-time data are backward looking, while patient screening and predicting future events are forward looking. The question we are asking is: can we use patient/plaque information from past and present to predict future? It is well established and validated by histopathological data that plaque ruptures are associated with very thin plaque cap, large necrotic lipid core, and extreme mechanical stress/strain conditions. However, for a plaque ruptured (or a patient who had a clinical event) at present, what was its morphology and mechanical conditions prior to the event? It is the information we can acquire prior to the event and their linkage to the event that could lead to possible predictions. The linkage between the plaque mechanical stress/strain conditions and clinical events is far from being established.

There is also an open question whether it is plaque wall stress, or flow shear stress that plays a more important role in the progression-rupture process. Arroyo and Lee (1999) provided an excellent a review of mechanical, biological and cellular factors concerning plaque initiation, progression and final rupture. We would like to emphasize that when performing predictive studies using in vivo patient data, we are facing more uncertainties and inaccuracies. Histology is often not available. The natural “gold standard” data (clinical events) is often hard to obtain. In this paper, we present the progress on image-based plaque modeling we made over the last decade with limited background review, emphasizing current challenging issues concerning vulnerable plaque models based on in vivo data. More complete reviews can be found from (Fleg et al., 2012; Richardson, 2002; Friedman et al., 2010).

2. Basic modeling elements, histology-based plaque classifications and a limited review

Computational modeling complements direct experimental measurements by providing flow shear stress and plaque stress/strain calculations which may be useful for better understanding and prediction of many critical biological processes. For computational

modelers, it is important to know the major elements involved in the modeling process so that they can formulate their models properly, and also know how closely they are modeling the actual physical and biological problems. The basic elements for image-based plaque models include (a) plaque morphology and components; (b) material properties of arteries and plaque components; (c) boundary conditions; (d) selection of model assumptions. It should be emphasized that many items needed for modeling are hard or near impossible to obtain in vivo, and are often subject to large errors when obtainable. Model construction procedures based on in vivo data are considerably different from earlier models based on idealized geometry or ex vivo data (Tang et al., 2004; Tang, 2006; Yang et al., 2007). Residual stress and zero-stress plaque morphology need to be handled properly to get accurate stress/strain predictions (Ohayon et al., 2007; Huang et al., 2009; Speelman et al., 2011).

A clearly thought-out *Data-Model-Prediction-Validation-Application* process will help us to understand the investigation process, design research projects and clarify the end points of the modeling effort. Direct modeling output (flow and stress/strain calculations) could be used to introduce plaque assessment scores, growth functions for plaque progression simulations, and as input for multiscale models to investigate the effect of mechanical forces on cellular activities.

2.1. Histology-based plaque classifications

One major difficulty in establishing and validating biomarkers for in vivo plaque assessment is lack of benchmarks based on in vivo data. Histology is viewed as the gold standard for image segmentation and model validation whenever the data are available. Stary et al. (1992, 1994, 1995) published a series of papers introducing histology-based American Heart Association (2005) plaque classifications: Type I lesions have microscopically detectable lipid deposits in the intima, some intimal thickening; Type II lesions: fatty streaks; Type III: pre-atheroma; Type IV: atheroma, the first lesion type considered as advanced; Type V: prominent new fibrous connective tissue has formed. Va: fibroatheroma, lipid core; Vb: lipid core and some calcified parts; Vc: a lipid core is absent and lipid in general is minimal; Type VI: “complicated” lesions, Type V lesions with disruptions of the lesion surface, hematoma or hemorrhage; Type VII: calcific lesions; Type VIII: fibrotic lesions with little or no lipid. While the AHA classification scheme has guided research efforts in the past 20 years, it is histology-based and is descriptive in nature. Virmani et al. (2000, 2006) provided more quantitative classifications for coronary and carotid atherosclerotic plaques based on extensive histological data and analysis. These works laid the foundation for further plaque assessment using other approaches. Of note, those histological studies indicated that large lipid-rich necrotic cores, very thin fibrous caps (a threshold value of 65 μm cap thickness was noted), lack of smooth muscle cells, and increased macrophage cells are all associated with plaque rupture and vulnerability.

2.2. The low flow shear stress hypothesis for early atherosclerosis initiation and progression

It is now well accepted that low and oscillating flow shear stresses correlate positively with intimal thickening and atherosclerosis progression (Ku et al., 1985; Friedman et al., 1987;

Friedman, 1993; Giddens et al., 1993; Nerem, 1992; Gibson et al., 1993). This “low flow shear stress (FSS)” hypothesis has dominated the atherosclerosis research field in recent years. More recently, in a multi-patient (n=20) intravascular ultrasound (IVUS)-based follow-up study, by dividing slices into low, intermediate, and high flow shear stress (FSS) groups and comparing the low and high FSS groups with the intermediate-FSS group, Samady et al. (2011) found that low-FSS segments demonstrated greater reduction in vessel ($P < 0.001$) and lumen area ($P < 0.001$), and high-FSS segments demonstrated an increase in vessel ($P < 0.001$) and lumen ($P < 0.001$) area . In a follow-up study of 506 patients with acute coronary syndrome (ACS) treated with a percutaneous coronary intervention and in a subset of 374 consecutive patients 6–10 months later to assess plaque natural history, Stone et al. (2012) reported that increase in plaque area was predicted by baseline large plaque burden; decrease in lumen area was independently predicted by baseline large plaque burden and low flow shear stress.

Several research groups reported findings controversial to the low FSS hypothesis and suggested the growing importance of searching for other mechanical factors such as plaque wall (structural) stresses (PWS) and new hypotheses for mechanisms governing plaque progression process (Joshi et al., 2004; Wentzel et al., 2005). In a follow-up study for patients undertaking lipid-lowering therapy (10 patients, 24 months follow-up), Wentzel et al. (2005) reported that flow shear stress did not predict plaque regression. The best predictor of plaque regression was baseline wall thickness. Using in vivo MRI of human carotid data, Tang et al. (2008) reported that 18 out of 21 patients showed negative correlations between human carotid atherosclerotic plaque progression and plaque wall stress at follow-up scan. In the PREDICTION study, Stone et al. (2012) also reported that plaque area was a good predictor of change in plaque area ($P < 0.001$), but flow shear stress was not a good predictor ($p = 0.32$) . Further investigations are needed to clarify the role of flow shear stress in plaque progression at advance stages.

2.3. 2D stress analysis for atherosclerotic vulnerable plaques

2D structure-only models were used by several authors to investigate stress/strain distributions in atherosclerotic plaques (Richardson et al., 1989; Cheng et al., 1993; Loree et al., 1992). Richardson et al. (1989) used atherosclerotic plaques from 85 patients who died from coronary thrombosis and investigated the characteristics of plaques which had fissured. Computer models were also constructed simulated the plaque morphologies with lipid composition. They reported that high circumferential stress correlated well with the site of intimal tears found at necropsy. Site of tearing was influenced by variation in the mechanical strength of cap tissue due to focal accumulation of foam cells and focal weak points in the cap which were not at the point of maximum stress. By using 24 human coronary artery lesions based on histological specimens, Cheng et al. (1993) reported that maximum circumferential stress in plaques that ruptured was significantly higher than maximum stress in stable specimens (544.9 ± 159.7 kPa versus 192.3 ± 64.6 kPa, $P < 0.0001$). Loree et al. (1992) investigated effects of fibrous cap and lipid pool on peak circumferential stress in atherosclerotic vessels and reported that plaque structural features such as thickness of the fibrous cap are more important factors in the distribution of stress in the plaque than stenosis severity. Huang et al. (2001) studied 20 human coronary lesions (10 ruptured and 10 stable)

and reported that maximum stress was not correlated with percentage of calcification, but it was positively correlated with the percentage of lipid ($p = 0.024$). Williamson et al. (2003) studied sensitivity of wall stresses in diseased arteries to material properties and reported that stresses within the arterial wall, fibrous plaque, calcified plaque, and lipid pool have low sensitivities to variations in the elastic modulus. Even a ± 50% variation in elastic modulus leads to less than a 10% change in stress at the site of rupture. Finet et al. used structural plaque models based on in vivo IVUS images of fibrous cap atheroma to investigate influence of plaque morphology, cap thickness and pressure loading on plaque stability. They considered a plaque as unstable if its plaque cap stress (PCS) was in excess of a threshold value of 300 kPa. They found that cap thickness <60 μm led to PCS > 300 kPa. PCS changes with plaque cap exponentially and slight change in plaque structure can change plaque stability (Finet et al., 2004). Ohayon et al. investigated the necrotic core thickness and arterial remodeling index as emergent biomechanical factors for evaluating the risk of plaque rupture. Twenty-four plaque data acquired by IVUS from patients and structural models were used to study the effect of anatomical plaque features on cap stress. They demonstrated that that plaque instability is to be viewed not as a consequence of fibrous cap thickness alone but rather as a combination of cap thickness, necrotic core thickness, and the arterial remodeling index (Ohayon et al., 2008). It should be noted that some of the conclusions from 2D models may need to be modified when 3D models are used and the plaque component size becomes large enough to affect stress/strain distributions. Still, these early work covered almost every aspect of plaque stress analysis and laid good foundation for further 3D image-based modeling investigations.

2.4. Additional modeling contributions for plaque stress/strain calculations

With evidence that higher plaque stresses are linked to plaque rupture and the selection of critical stress value as the representative value, critical stress values have been used in several studies concerning plaque rupture and assessment. Vengrenyuk et al. (2006, 2008), Bluestein et al. (2008), Maldonado et al. (2012), Cardoso and Weinbaum (2013), and Kelly-Arnold et al. (2013) demonstrated that plaque cap with micro-calcification inclusions are associated with elevated stress levels and may be related to plaque rupture. Gao et al. (2011) studied carotid plaques and found that critical stress values from symptomatic patients were higher that from asymptomatic patients. Intraplaque hemorrhage has been found to be closely related to potential plaque rupture (Underhill et al., 2010). Huang et al. (2012) performed a multi-patient modeling study and found that locations of intraplaque hemorrhages corresponded to higher stress values than non-hemorrhage locations. Holzapfel et al. (2002) introduced a multilayer anisotropic 3D model for a human external iliac artery with eight distinct arterial components associated with specific mechanical responses. The multi-layer anisotropic model was compared with some simplified models (neglecting axial in situ pre-stretch, assuming plane strain states, and isotropic material responses), and maximum stress deviations of up to 600% were found. Steinman (2002) and Lee et al. (2008) investigated effects of plaque geometrical features on flow behaviors using realistic plaque geometries. By using patient-specific plaque data, they indicated that plaque geometrical features have considerable impact on flow shear stress which is closed related to plaque progression and rupture processes.

2.5. Quantification of plaque material properties using imaging data

It is believed that vessel and plaque material properties have considerable influence on plaque stress/strain conditions and stability. Quantifying tissue material properties based on in vivo data is challenging. Le Floc'h et al. (2012) and Baldewsing et al. (2008) have conducted research to reconstruct in vivo vulnerable plaque (VP) elasticity. A four-criterion selection procedure was proposed for plaque elasticity reconstruction based on in vivo coronary IVUS radial strain sequences and was tested on data obtained from 12 patients (Le Floc'h et al., 2012). As it is known that plaque has heterogeneous morphology and local material property is needed to have accurate stress/strain calculations, Baldewsing et al. introduced an inverse method for imaging the local plaque elasticity. The method was tested using both ex vivo and in vivo human coronary plaque samples (Baldewsing, et al., 2008). Liu et al. introduced a method based on human CINE MRI carotid data and computational modeling to determined plaque material parameters (Liu et al., 2012b). Data from 12 patients were used. Plaque material parameters as well as shrinkage rate (from in vivo shape to zero pressure shape) were determined. It was found that the stiffness of the samples may vary by as much as 1000% (Young's moduli ranged from 137.2 kPa to 1435.9 kPa). Vessel stiffness variation up to 100% had very little effect on stress (< 5%) when pre-shrink process was applied.

3. In vivo image-based FSI models for atherosclerotic vulnerable plaques

3.1. Basic techniques concerning FSI plaque modeling based on in vivo data

While many researchers are familiar with the general procedures for image-based modeling with fluid–structure interactions, some new techniques concerning modeling using in vivo data have considerable impact on computational stress/strain predictions, and their importance should be better recognized. Three specific techniques in constructing patient-specific 3D FSI multi-component models based on in vivo are worth mentioning: (a) pre-shrink–stretch process to handle residual stress issue; (b) component-fitting technique to build mesh with multi-components imbedded in the plaque structure; (c) cyclic bending for coronary modeling simulating heart motion.

3.1.1. Pre-shrink–stretch process and residual stress—It is well known that residual stress has considerable effect on stress/strain calculations (Ohayon et al., 2007; Speelman et al., 2011). In vivo plaque morphology data are acquired when the vessel is under physiological pressure, stretch and other tethering forces. To make an accurate prediction of wall stress/strain requires knowledge of the zero pressure stress distributions. A shrink–stretch process is needed (see Fig. 1) (Tang, 2006; Huang et al., 2009) to (a) shrink in vivo plaque geometry to obtain a starting no-load geometry; and (b) apply pressure and axial stretch to recover original in vivo geometry with residual stress/strain computed. The shrinking rate in the axial direction and shrinkage rates of lumen and outer wall (which have to be different) were determined so that (1) mass conservation is satisfied; and (2) the contours of the plaque and its components after pressurization and axial stretch achieve the best match with the in vivo geometry from MRI. A circular artery segment under in vivo condition goes through three stages to get its open-up zero-stress state: axial shrinkage (up to 30–50%; could be smaller for atherosclerotic plaques), circumferential shrinkage (5–20%

based on our data, Huang et al., 2009; Liu et al., 2012b), and final opening-up with an opening angle (63.5°, $n = 5$) (Kural et al., 2012). Omitting any of the three stages would lead to stress/strain prediction errors on the order of 50–100% or even more (Liu et al., 2012b; Huang et al., 2009; Ohayon et al., 2007). Ohayon et al. (2007) investigated the influence of residual stress/strain related to opening angle on the biomechanical stability of vulnerable coronary plaques and their potential impact for evaluating the risk of plaque rupture. Huang et al. (2009) quantified the axial and circumferential shrinkage for human carotid arteries by comparing ex vivo and in vivo MRI data from 10 patients. Speelman et al. (2011) introduced an inverse method to address the initial stress in biomechanical models of atherosclerotic plaques. The inverse method was more sophisticated compared to the direct trial-and-error iterative shrinkage identification process used in our papers (Huang et al., 2009; Liu et al., 2012b). Actually, even including all the three stages for computational models would still not be able to account for plaque local plaque material and morphology variations. In vivo local plaque information would be needed to come up with more accurate models with zero-stress issue better addressed. All of these require considerable effort and data are normally not available in vivo. A balance between ultimate accuracy and available data and resources should be kept when making modeling assumptions.

3.1.2. Component-fitting mesh generation technique—Because plaques using FSI models have complex irregular deformable geometries with component inclusions which are challenging for mesh generation, Yang et al. (2009) and Huang et al. (2009) developed a component-fitting mesh generation technique for multi-component plaque FSI models. The technique is simple but labor intensive. Fig. 2 gives an illustration of the method. Using this technique, the 3D plaque domain was divided into hundreds of small volumes to fit the irregular plaque geometry with component inclusions. A mesh for each small volume was then generated. With meshes generated by this technique, convergence of the fully coupled FSI models could be achieved with modest effort. Other groups have developed more sophisticated adaptive and automatic mesh generation techniques using octree-based isocontouring method to construct unstructured 3D meshes for a single-material (homogeneous) domain with manifold boundary. The method was further extended to handle multi-materials by using a material change edge to identify the interface between two or several different materials. Details of those methods can be found from Zhang et al. (2005) and Zhang et al. (2010).

3.1.3. Cyclic bending in coronary plaque modeling and its impact on stress predictions—One distinguishing feature for coronary plaque modeling is its cyclic bending caused by heart contraction. Yang et al. introduced the first patient-specific in vivo IVUS-based coronary plaque model with (a) fluid–structure interaction; (b) anisotropic vessel material properties; (c) cyclic bending of the coronary caused by heart motion (Tang et al., 2009c; Yang et al., 2009, Liu et al., 2012a). Fig. 3 used one coronary sample to demonstrate IVUS data, segmented contours and re-constructed 3D vessel geometry of a coronary segment. Angiography was used to determine vessel curvature and curvature variations. Fig. 4 give plots of plaque wall stresses and flow shear stresses from four models to illustrate the impact of cyclic bending and anisotropic properties on PWS and FSS distributions: Model 1 (M1), anisotropic model with cyclic bending and pulsating pressure;

Model 2 (M2), same as M1, but no bending; Model 3 (M3), isotropic model, no bending; Model 4 is the same as M1, but with 10% axial stretch. Taking M3 as the base model, maximum PWS values on the cut-surface (at maximum bending where applicable) from M2, M1 and M4 were 63%, 126%, and 345% higher, respectively. The increases for plaque wall strain (PWSn) were even higher at 104%, 278%, and 391%, respectively. Cyclic bending caused a modest 15% decrease in maximum FSS, 5% decrease in maximum velocity, and 8.7% decrease in flow rate (99.0 ml/min from M1 vs. 108.4 ml/min from M2).

Ohayon et al. (2011) also included heart contraction in their multi-patient coronary plaque study using 3D structural models based on in vivo CT (for morphology) and MRI (for ventricle contraction). Data from eight patients were used in their study. Their models included left main coronaries with bifurcation. Centerlines of coronary arteries were determined from CT scans while circular cross sections and uniform wall thickness were assumed in their models. Cardiac motion was imposed on the adventitia region of the vessel in contact with myocardium. Structural static finite element (FE) computations were performed to obtain stress/strain distributions. They found that all plaque sites were concomitantly subject to high luminal arterial wall stretch ($LW_{Stretch}$) and high luminal arterial wall stiffness (LW_{Stiff}), with mean amplitudes of 34.7 ± 1.6% and 442.4 ± 113.0 kPa, respectively. Their findings suggest that local wall stiffness plays a role in the initiation of atherosclerotic lesions.

3.2. Predictive risk factors and indices for plaque classification and rupture prediction

Since plaque rupture occurs when the mechanical stress in the plaque exceeds the ultimate strength of the plaque cap material, it is natural to expect that plaque rupture may be associated with extreme mechanical stress/strain conditions. In this connection, several issues have to be addressed for in vivo modeling studies: (a) what can we use as the “gold standard” to establish the association between plaque rupture and mechanical factors using in vivo data? (b) Can mechanical stress/strain risk factors be used to *predict* plaque rupture and what are their predicting accuracies? (c) Can mechanical risk factors provide better predictions, compared to what we can get by using morphological features alone? (d) How can mechanical stress/strain be used to introduce new plaque vulnerability indices for improved plaque classifications? Some preliminary work is provided as motivations for further effort and discussions.

3.2.1. In vivo evidence that plaque rupture is associated with higher critical plaque stress—For carotid plaques, magnetic resonance imaging (MRI) is currently the best imaging modality providing plaque morphology and component differentiations (lipid-rich necrotic core, calcification, hemorrhage, ulceration, etc.) (Yuan et al., 2001a; Underhill et al., 2010). In seeking in vivo evidence that plaque rupture is associated with mechanical forces, Tang et al. (2009b) and Teng et al. (2010) used plaques with ulceration as a benchmark and compared their critical PWS values for plaques without ulcerations. Figs. 5 and 6 demonstrate a plaque example with rupture where critical plaque wall stress (CPWS) was able to predict site of rupture. CPWS is defined as the maximum of all plaque maximum principal stress values at vulnerable sites such as a site where a thin fibrous cap covers a large lipid core (Tang et al., 2009b).

Table 1 shows that the mean 3D CPWS of plaques with ulceration (Group 1) was 263.44 kPa which was 100% higher than that from plaques without ulceration (Group 2, 132.77 kPa, p=0.03984). Five of the six ruptured plaques had 3D CPWS sites, matching the histology confirmed rupture sites, with an 83% agreement. Although the mean 3D CFSS (92.94 dyn/cm^2) for Group 1 was 76% higher than that for Group 2 (52.70 dyn/cm^2), only two of the six ruptured plaques had 3D CFSS sites matching the histology-confirmed rupture sites, with a 33% agreement.

3.2.2. Stress-based indices for plaque vulnerability and classifications—To identify and introduce potential plaque vulnerability indices, we need to (a) identify the risk factors; (b) choose representative values for those factors; (c) establish linkage between those values (indices) and plaque vulnerability; (d) validate the linkage. Tang et al. (2005) indicated that critical plaque wall stress (CPWS) is associated with plaque rupture and may be used for plaque assessment. Critical plaque wall stress was defined as the largest local maxima of plaque wall stresses (maximum principal stresses) from all possible vulnerable sites of the plaque (Tang et al., 2005, 2009b). Possible vulnerable sites of a plaque include all sites with local stress/strain maxima, especially where a thin cap was covering a lipid core, but exclude healthy sites where rupture is unlikely, even if a local stress maximum occurred there. Our stress-based plaque assessment had 85% agreement rate with histopathological plaque vulnerability index (HPVI) for coronary plaques (34 2D samples, Figs. 7 and 8) and 80.1% agreement rate with in vivo morphological plaque vulnerability index (MPVI, see Table 2) for carotid plaques (206 2D samples) (Tang et al., 2005, 2009a). HPVI and MPVI were defined based on factors related to plaque vulnerability including cap thickness, lipid core size, hemorrhage and inflammation, and other factors. Table 3 gives CPVI scores for 152 in vivo MRI slices, as well as their AHA classifications based on morphological features. Sixty-two slices out of 99 Type V received CPVI score 2 or less. Twelve slices out of 32 Type VI slices received score 2 or less. Since CPVI could further divide plaques of the same AHA classes, which is an indication that CPVI may complement AHA classifications and provided potential improvement for plaque assessment (Tang et al., 2009a).

3.2.3. Predictive method and accuracy of prediction—Most investigations for atherosclerotic plaque progression and rupture have focused on correlation studies between risk factors and potential events (progression, rupture, stroke, and heart attack). However, it is far more important and of more practical significance that we develop methods which can predict the critical clinical events before their actual occurrence. In our recent paper (Wu et al., 2011), a predictive method was introduced where 3D FSI models were constructed based on patient data with follow-up scan showing ulceration indicating plaque rupture (Fig. 9). Plaque wall stress (PWS) and strain (PWSn) and flow maximum shear stress (FSS) were extracted from all 600 matched nodal points (100 points per matched slice, baseline matching follow-up) on the lumen surface for analysis. Each of the 600 points was marked “ulcer” or “non-ulcer” using follow-up scan. Predictive statistical models for each of the seven combinations of PWS, PWSn and FSS were trained using the follow-up data and applied to the baseline data to assess their sensitivity and specificity using the 600 data points for ulcer predictions. Using probability 0.3 as a threshold to infer ulcer occurrence at

the prediction stage, Table 4 shows the combination of PWS and PWSn provided the best predictive accuracy with (sensitivity, specificity) = (0.97, 0.958). The method could be applied at population level to identify the optimal predictor(s) for plaque rupture or selected specific clinical observations.

While the above paper was to predict which node at baseline would likely become an ulcer node, the method can be applied to multi-patients to predict at patient level that which patient is likely to have plaque rupture or a clinical event. The challenge is: it is extremely difficult to obtain patient data with enough number of ruptures or events to train and validate the models.

3.3. Mechanisms governing advanced carotid and coronary plaque progression

Some important contributions were covered in Section 2.2. Using patient-specific in vivo carotid MRI data from 14 patients and 32 scan pairs (baseline—follow up, see Fig. 10) and 3D FSI models, we found that 21 out of the 32 scan pairs showed a significant positive correlation between plaque progression and FSS at follow-up, and 26 out of 32 scan pairs showed a significant negative correlation between plaque progression and plaque wall stress at follow-up (Yang et al., 2010). Most patients changed correlation signs from one period to another period. Use of lipid-lowering medication may be a possible cause for the change.

4. Grand challenges: data, model, validation, and patient screening

4.1. New development and challenges in MRI technology

MRI has been extensively used to render 3D vessel geometry and plaque composition needed to compute patient-specific mechanical stress distribution which could be responsible for atherosclerotic plaque rupture. Recent advances in MRI technology are allowing MRI to be used as a tool to overcome the limitations of the numerical models by either improving the boundary conditions and assumptions on material properties, or estimating in vivo blood flow and vessel wall deformation measurements (Canton et al., 2012; Harloff et al., 2009a, 2009b; Lin et al., 2008). Markl and collaborators have proved the feasibility of time-resolved gated cine PC-MRI with three-directional encoding, known as 4D flow MRI, to characterize flow patterns in different arterial segments (Markl et al., 2010; Harloff, et al., 2009a), indicating that PC-MRI could emerge as a potential gold standard technique for in vivo measuring the spatial distribution of velocity field. However, the major challenge of 4D flow MRI is to obtain detailed measurement of the time-varying velocity near the wall in the branching and curved arteries where atherosclerosis develops, where the flow can be highly skewed; or in stenotic regions where the lumen is not circular. Moreover, faster imaging sequences and inexpensive imaging equipment would be clearly needed before in vivo PC-MRI flow characterization of the diseased artery can become part of routine clinical practice.

Atherosclerosis decreases arterial wall elasticity due to the release of nitric oxide triggered by endothelial dysfunction. The arterial elasticity is further decreased by risk factors associated to atherosclerosis such as hypertension and diabetes. This decrease in elasticity directly affects the arterial wall cyclic strain. MR DENSE pulse sequence has been used to provide the circumferential strain distribution (Lin et al., 2008) whereas gated cine MRI has

been used to measure arterial wall distensibility. Although these MR techniques used in higher field strength of 3 T scanners have been shown to be a promising tool to measure strain and distensibility due to its substantially increase of the signal-to-noise, further increase of spatial and temporal resolution is still needed to provide reliable measurements in diseased carotid arteries (Harloff et al., 2009b). Furthermore, prospective studies are still required to investigate in depth the complex interplay of hemodynamic forces and the pathological processes leading to disease progression.

4.2. IVUS, optical coherence tomography (OCT) and near infrared spectroscopy (NIRS)

The accuracy and reliability of image-based modeling are ultimately determined by the quality and accuracy of medical images available to the modelers and a better understanding of imaging parameters will be helpful to biomechanical modelers. As described above, our current understanding of atherosclerotic CAD suggests that the risk of death and future adverse events is related to the extent and characteristics of coronary plaque and its interaction with blood flow. Traditional prediction of risk and, often, determination of therapy, for patients with CAD has relied on inherently limited imaging modalities, such as coronary angiography. In distinction, the emergence of IVUS for imaging of coronary vessels and atherosclerotic plaque has allowed more precise definition of vessel, lumen, and plaque characteristics, including serial assessment for natural history (progression-regression) and intervention studies (restenosis in both stented and non-stented lesions).

However, one of the fundamental limitations of grayscale IVUS is related to assessment of plaque composition. More advanced signal analysis (Virtual Histology, VH-IVUS; Volcano Therapeutics) using both envelope amplitude of the reflected radiofrequency signals and frequency content has allowed spectral imaging to resolve distinct tissue components of atherosclerotic plaques. While VH-IVUS has provided unique perspectives on in vivo human atherosclerotic plaque and novel insights into plaque morphology and natural history (Stone et al., 2011; Stone and Mintz, 2010), there remain several challenges that may limit the application of VH-IVUS to fully assess complete plaque composition and geometry: (1) it remains an invasive modality with catheter diameters in the 1 mm range, with associated risks and limitations on its application for plaques causing very severe luminal narrowing; (2) in the automated analysis a medial layer is artificially added on the borderline of the outer vessel volume; (3) no thrombus or intra-plaque hemorrhage can be reliably identified, which is a disadvantage for the assessment of vulnerable or ruptured plaques; (4) there is still limited resolution (50–100 μm) that may prevent delineation of very thin caps (< 40 μm); and (5) there are issues raised about reliability of VH IVUS in quantifying individual plaque components. Thim et al. used adult atherosclerosis-prone minipigs in their study and 18 advanced coronary lesions were assessed by VH IVUS in vivo followed by postmortem microscopic examination (histology). They found no correlation between the size of the necrotic core determined by VH IVUS and histology (Thim et al., 2010). Stone and Mintz commented that the lack of correlation Thim et al. reported may be caused by difficulty in matching histology and VH IVUS sections, technical handling of data, individual differences of pathologists, and other factors (Stone and Mintz, 2010).

The application and integration of additional and potentially complementary intravascular imaging methods, such as optical coherence tomography (OCT) and near infrared spectroscopy (NIRS), among other emerging vascular imaging technologies that include high-definition IVUS, may help advance our ability to diagnose vulnerable from non-vulnerable plaques to enhance future risk prediction and effective treatment for patients with CAD (Tearney et al., 2012; Caplan et al., 2006; Gardner et al., 2008; Maehara et al., 2013; Bourantas et al., 2013). OCT uses light rather than ultrasound, has a resolution of 15–20 μm and therefore can measure fibrous cap thickness, can classify plaque as fatty, fibrotic, calcific, or thrombotic; and can detect thin-cap fibroatheromas and plaque erosions in patients presenting with an acute coronary syndrome. The major limitations of OCT are penetration so that overall plaque burden cannot be measured and the inability to image through blood or penetrate red thrombus. NIRS was developed specifically to detect lipid within the vessel wall; in the first combined intravascular imaging device, it has been paired with IVUS in a single catheter. NIRS also uses an optic fiber to transmit and receive NIR light (wave length 0.8–2.5 μm) into the tissue. The pattern of absorption of the light in relation to the wave length is unique for lipid. There is a potential that algorithms could be developed to assess the presence of a fibrous cap within lipid-rich necrotic lesions which could allow detection of vulnerable plaques. Caution should be exercised before more evidence and progress could be shown for the potential of the new NIRS applications in vulnerable plaque detection.

4.3. Predictive methods, screening, and real life demand as motivation

We are aware that our data are not accurate; our models do not match the real physics entirely; and our predictions may have no or little validations (we may sincerely believe that our plaque assessment scores make sense). However, as accurate predictive methods have not been established yet, when a patient walks into a clinic, the physician has to decide about what (s)he can do to treat the patient, based on the information (s)he could get with available technologies. This is the challenge we are facing. We have to do our best to provide the best treatment per our judgment, while we continue to improve our methods and technologies.

Acknowledgments

This research was supported in part by NSF Grant DMS-0540684, NIH/NIBIB 2R01EB004759, and NIH R01 HL073401. Professor Chun Yang's research was partially supported by National Natural Sciences Foundation of China Grant 11171030. Dr. Xueying Huang's research was partially supported by National Natural Sciences Foundation of China Grant 31100670.

References

American Heart Association. Heart Disease and Stroke Statistics–2005 Update. 2005. http://www.americanheart.org/downloadable/heart/1105390918119-HDSStats2005Update.p

Arroyo LH, Lee RT. Mechanisms of plaque rupture: mechanical and biologic interactions. Cardiovasc Res. 1999; 41(2):369–375. [PubMed: 10341836]

Baldewsing RA, Danilouchkine MG, Mastik F, Schaa JA, Serruys PW, van der Steen AF. An inverse method for imaging the local elasticity of atherosclerotic coronary plaques. IEEE Trans Inf Technol Biomed. 2008; 12(3):277–289. [PubMed: 18693495]

Barnett HJ, Eliasziw M, Meldrum HE. Evidence based cardiology: prevention of ischaemic stroke. Br Med J. 1999; 318(7197):1539–1543. [PubMed: 10356014]

Bluestein D, Alemu Y, Avrahami I, Gharib M, Dumont K, Ricotta JJ, Einav S. Influence of microcalcifications on vulnerable plaque mechanics using FSI modeling. J Biomech. 2008; 41(5): 1111–1118. [PubMed: 18258240]

Bourantas CV, Garcia-Garcia HM, Farooq V, Maehara A, Xu K, Généreux P, Diletti R, Muramatsu T, Fahy M, Weisz G, Stone GW, Serruys PW. Clinical and angiographic characteristics of patients likely to have vulnerable plaques: analysis from the PROSPECT study. JACC Cardiovasc Imaging. 2013; 6(12):1263–1272. [PubMed: 24269259]

Canton G, Hippe DS, Sun J, Kerwin WS, Tang D, Yuan C. Characterization of distensibility, plaque burden and composition of the atherosclerotic carotid artery using magnetic resonance imaging. Med Phys. 2012; 39(10):6247–6254. [PubMed: 23039660]

Caplan JD, Waxman S, Nesto RW, Muller JE. Near-infrared spectroscopy for the detection of vulnerable coronary artery plaques. J Am Coll Cardiol. 2006; 47(8 Suppl):C92–C96. [PubMed: 16631516]

Cardoso L, Weinbaum S. Changing views of the biomechanics of vulnerable plaque rupture: a review. Ann Biomed Eng. 2013 [Epub ahead of print]. [PubMed - as supplied by publisher]. [PubMed: 23842694]

Cheng GC, Loree HM, Kamm RD, Fishbein MC, Lee RT. Distribution of circumferential stress in ruptured and stable atherosclerotic lesions. A structural analysis with histopathological correlation. Circulation. 1993; 87:1179–1187. [PubMed: 8462145]

Finet G, Ohayon J, Rioufol G. Biomechanical interaction between cap thickness, lipid core composition and blood pressure in vulnerable coronary plaque: impact on stability or instability. Coron Artery Dis. 2004; 15(1):13–20. [PubMed: 15201616]

Fleg JL, Stone GW, Fayad ZA, Granada JF, Hatsukami TS, Kolodgie FD, Ohayon J, Pettigrew R, Sabatine MS, Tearney GJ, Waxman S, Domanski MJ, Srinivas PR, Narula J. Detection of high-risk atherosclerotic plaque: report of the NHLBI working group on current status and future directions. JACC Cardio Imaging. 2012; 5(9):941–955.

Friedman MH. Arteriosclerosis research using vascular flow models: from 2-D branches to compliant replicas. J Biomech Eng. 1993; 115:595–601. [PubMed: 8302047]

Friedman MH, Bargeron CB, Deters OJ, Hutchins GM, Mark FF. Correlation between wall shear and intimal thickness at a coronary artery branch. Atherosclerosis. 1987; 68:27–33. [PubMed: 3689481]

Friedman MH, Krams R, Chandran KB. Flow interactions with cells and tissues: cardiovascular flows and fluid–structure interactions. Ann Biomed Eng. 2010; 38(3):1178–1187. [PubMed: 20336826]

Fuster, V. The vulnerable atherosclerotic plaque: understanding, identification, and modification. In: Fuster; Valentin; Cornhill, JF.; Dinsmore, RE.; Fallon, JT.; Insull, W.; Libby, P.; Nissen, S.; Rosenfeld, ME.; Wagner, WD., editors. AHA Monograph Series. Futura Publishing; Armonk, NY: 1998.

Fuster V, Stein B, Ambrose JA, Badimon L, Badimon JJ, Chesebro JH. Atherosclerotic plaque rupture and thrombosis, evolving concept. Circulation. 1990; 82:SII-47–59.

Gao H, Long Q, Das SK, Halls J, Graves M, Gillard JH, Li ZY. Study of carotid arterial plaque stress for symptomatic and asymptomatic patients. J Biomech. 2011; 44(14):2551–2557. [PubMed: 21824619]

Gardner CM, Tan H, Hull EL, Lisauskas JB, Sum ST, Meese TM, Jiang C, Madden SP, Caplan JD, Burke AP, Virmani R, Goldstein J, Muller JE. Detection of lipid core coronary plaques in autopsy specimens with a novel catheter-based near-infrared spectroscopy system. JACC Cardiovasc Imaging. 2008; 1(5):638–648. [PubMed: 19356494]

Garrett, MF.; Laird, NM.; Ware, JH. Applied Longitudinal Analysis. Wiley-Interscience; Hoboken, NJ: 2004.

Gibson CM, Diaz L, Kandarpa K, Sacks FM, Pasternak RC, Sandor T, Feldman C, Stone PH. Relation of vessel wall shear stress to atherosclerosis progression in human coronary arteries. Arterioscler Thromb Vasc Biol. 1993; 13(2):310–315.

Giddens DP, Zarins CK, Glagov S. The role of fluid mechanics in the localization and detection of atherosclerosis. J Biomech Eng. 1993; 115:588–594. [PubMed: 8302046]

Gorelick PB. Carotid endarterectomy: where do we draw the line? Stroke. 1990; 30:1745–1750. [PubMed: 10471418]

Harloff A, Albrecht F, Spreer J, Stalder AF, Bock J, Frydrychowicz A, Schöllhorn J, Hetzel A, Schumacher M, Hennig J, Markl M. 3D blood flow characteristics in the carotid artery bifurcation assessed by flow-sensitive 4D MRI at 3 T. Magn Reson Med. 2009a; 61(1):65–74. [PubMed: 19097219]

Harloff A, Zech T, Frydrychowicz A, Schumacher M, Schöllhorn J, Hennig J, Weiller C, Markl M. Carotid intima-media thickness and distensibility measured by MRI at 3 T versus high-resolution ultrasound. Eur Radiol. 2009b; 19(6):1470–1479. [PubMed: 19214524]

Holzapfel GA, Stadler M, Schulze-Bause CAJ. A layer-specific three-dimensional model for the simulation of balloon angioplasty using Magnetic Resonance Imaging and mechanical testing. Ann Biomed Eng. 2002; 30(6):753–767. [PubMed: 12220076]

Huang H, Virmani R, Younis H, Burke AP, Kamm RD, Lee RT. The impact of calcification on the biomechanical stability of atherosclerotic plaques. Circulation. 2001; 103:1051–1056. [PubMed: 11222465]

Huang X, Yang C, Canton G, Ferguson M, Yuan C, Tang D. Quantifying effect of intraplaque hemorrhage on critical plaque wall stress in human atherosclerotic plaques using 3D FSI models. J Biomech Eng. 2012; 134(12):121004. [PubMed: 23363206]

Huang X, Yang C, Yuan C, Liu F, Canton G, Zheng J, Woodard PK, Sicard GA, Tang D. Patient-specific artery shrinkage and 3D zero-stress state in multi-component 3D FSI models for carotid atherosclerotic plaques based on in vivo MRI data. Mol Cell Biomech. 2009; 6(2):121–134. [PubMed: 19444328]

Joshi AK, Leask RL, Myers JG, Ojha M, Butany J, Ethier CR. Intimal thickness is not associated with wall shear stress patterns in the human right coronary artery. Arterioscler Thromb Vasc Biol. 2004; 24(12):2408–2413. [PubMed: 15472129]

Kelly-Arnold A, Maldonado N, Laudier D, Aikawa E, Cardoso L, Weinbaum S. Revised microcalcification hypothesis for fibrous cap rupture in human coronary arteries. Proc Natl Acad Sci USA. 2013; 110(26):10741–10746. [PubMed: 23733926]

Ku DN, Giddens DP, Zarins CK, Glagov S. Pulsatile flow and atherosclerosis in the human carotid bifurcation: positive correlation between plaque location and low and oscillating shear stress. Arteriosclerosis. 1985; 5:293–302. [PubMed: 3994585]

Kural MH, Cai MC, Tang D, Gwyther T, Zheng J, Billiar KL. Planar biaxial characterization of diseased human coronary and carotid arteries for computational modeling. J Biomech. 2012; 45(5):790–798. [PubMed: 22236530]

Le Floc'h S, Cloutier G, Saijo Y, Finet G, Yazdani SK, Deleaval F, Rioufol G, Pettigrew RI, Ohayon J. A four-criterion selection procedure for atherosclerotic plaque elasticity reconstruction based on in vivo coronary intravascular ultrasound radial strain sequences. Ultrasound Med Biol. 2012; 38(12):2084–2097. [PubMed: 23196202]

Lee SW, Antiga L, Spence JD, Steinman DA. Geometry of the carotid bifurcation predicts its exposure to disturbed flow. Stroke. 2008; 39(8):2341–2347. [PubMed: 18556585]

Lin AP, Bennett E, Wisk LE, Gharib M, Fraser SE, Wen H. Circumferential strain in the wall of the common carotid artery: Comparing displacement-encoded and cine MRI in volunteers. Magn Reson Med. 2008; 60(1):8–13. [PubMed: 18581403]

Liu H, Cai M, Yang C, Zheng J, Bach R, Kural MH, Billiar KL, Muccigrosso D, Lu D, Tang D. IVUS-based computational modeling and planar biaxial artery material properties for human coronary plaque vulnerability assessment. Mol Cell Biomech. 2012a; 9:77–93. [PubMed: 22428362]

Liu HF, Canton G, Yuan C, Yang C, Billiar KL, Teng ZZ, Hoffman AH, Tang D. Using in vivo Cine and 3D multi-contrast MRI to determine human atherosclerotic carotid artery material properties and circumferential shrinkage rate and their impact on stress/strain predictions. J Biomech Eng. 2012b; 134(1):011008. [PubMed: 22482663]

Loree HM, Kamm RD, Stringfellow RG, Lee RT. Effects of fibrous cap thickness on peak circumferential stress in model atherosclerotic vessels. Circ Res. 1992; 71:850–858. [PubMed: 1516158]

Maehara A, Mintz GS, Stone GW. OCT versus IVUS: accuracy versus clinical utility. JACC Cardiovasc Imaging. 2013; 6(10):1105. [PubMed: 24135323]

Maldonado N, Kelly-Arnold A, Vengrenyuk Y, Laudier D, Fallon JT, Virmani R, Cardoso L, Weinbaum S. A mechanistic analysis of the role of micro-calcifications in atherosclerotic plaque stability: potential implications for plaque rupture. Am J Physiol Heart Circ Physiol. 2012; 303(5):H619–H628. [PubMed: 22777419]

Markl M, Wegent F, Zech T, Bauer S, Strecker C, Schumacher M, Weiller C, Hennig J, Harloff A. In vivo wall shear stress distribution in the carotid artery effect of bifurcation geometry, internal carotid artery stenosis, and recanalization therapy. Circ-Cardiovasc Imaging. 2010; 3:647–655. [PubMed: 20847189]

Naghavi M, Libby P, Falk E, Casscells SW, Litovsky S, Rumberger J, Badimon JJ, Stefanadis C, Moreno P, Pasterkamp G, Fayad Z, Stone PH, Waxman S, Raggi P, Madjid M, Zarrabi A, Burke A, Yuan C, Fitzgerald PJ, Siscovick DS, de Korte CL, Aikawa M, Juhani Airaksinen KE, Assmann G, Becker CR, Chesebro JH, Farb A, Galis ZS, Jackson C, Jang IK, Koenig W, Lodder RA, March K, Demirovic J, Navab M, Priori SG, Rekhter MD, Bahr R, Grundy SM, Mehran R, Colombo A, Boerwinkle E, Ballantyne C, Insull W, Schwartz RS, Vogel R, Serruys PW, Hansson GK, Faxon DP, Kaul S, Drexler H, Greenland P, Muller JE, Virmani R, Ridker PM, Zipes DP, Shah PK, Willerson JT. From vulnerable plaque to vulnerable patient: a call for new definitions and risk assessment strategies: Part I. Circulation. 2003a; 108(14):1664–1672. [PubMed: 14530185]

Naghavi M, et al. From vulnerable plaque to vulnerable patient: a call for new definitions and risk assessment strategies: Part II. Circulation. 2003b; 108(15):1772–1778. [PubMed: 14557340]

Nerem RM. Vascular fluid mechanics, the arterial wall, and atherosclerosis. J Biomech Eng. 1992; 114:274–282. [PubMed: 1522720]

Ohayon J, Dubreuil O, Tracqui P, Floc'h SL, Rioufol G, Chalabreysse L, Thivolet F, Pettigrew RI, Finet G. Influence of residual stress/strain on the biomechanical stability of vulnerable coronary plaques: potential impact for evaluating the risk of plaque rupture. Am J of Physiol Heart Circ Physiol. 2007; 293:H1987–H1996. [PubMed: 17604326]

Ohayon J, Finet G, Gharib AM, Herzka DA, Tracqui P, Heroux J, Rioufol G, Kotys MS, Elagha A, Pettigrew RI. Necrotic core thickness and positive arterial remodeling index: emergent biomechanical factors for evaluating the risk of plaque rupture. Am J Physiol Heart Circ Physiol. 2008; 295(2):H717–H727. [PubMed: 18586893]

Ohayon J, Gharib AM, Garcia A, Heroux J, Yazdani SK, Malvè M, Tracqui P, Martinez MA, Doblare M, Finet G, Pettigrew RI. Is arterial wall-strain stiffening an additional process responsible for atherosclerosis in coronary bifurcations? An in vivo study based on dynamic CT and MRI. Am J Physiol Heart Circ Physiol. 2011; 301(3):H1097–H1106. [PubMed: 21685261]

Richardson PD. Biomechanics of plaque rupture: progress, problems, and new frontiers. Ann Biomed Eng. 2002; 30(4):524–536. [PubMed: 12086003]

Richardson PD, Davies MJ, Born GV. Influence of plaque configuration and stress distribution on fissuring of coronary atherosclerotic plaques. Lancet. 1989; 2(8669):941–944. [PubMed: 2571862]

Samady H, Eshtehardi P, McDaniel MC, Suo J, Dhawan SS, Maynard C, Timmins LH, Quyyumi AA, Giddens DP. Coronary artery wall shear stress is associated with progression and transformation of atherosclerotic plaque and arterial remodeling in patients with coronary artery disease. Circulation. 2011; 124(7):779–788. [PubMed: 21788584]

Speelman L, Akyildiz AC, den Adel B, Wentzel JJ, van der Steen AF, Virmani R, van der Weerd L, Jukema JW, Poelmann RE, van Brummelen EH, Gijsen FJ. Initial stress in biomechanical models of atherosclerotic plaques. J Biomech. 2011; 44(13):2376–2382. [PubMed: 21782179]

Stary HC, Blankenhorn DH, Chandler AB, Glagov S, Insull W, Richardson M, Rosenfeld ME, Schaffer SA, Schwartz CJ, Wagner WD, Wissler RW. A definition of the intima of human arteries and of its atherosclerosis-prone regions. A report from the Committee on Vascular Lesions of the Council on Arteriosclerosis, AHA. Circulation. 1992; 85:391–405. [PubMed: 1728483]

Stary HC, Chandler AB, Glagov S, Guyton JR, Insull W, Rosenfeld ME, Schaffer SA, Schwartz CJ, Wagner WD, Wissler RW. A definition of initial, fatty streak and intermediate lesions of atherosclerosis. A report from the Committee on Vascular Lesions of the Council on Arteriosclerosis, AHA. Circulation. 1994; 89:2462–2478. [PubMed: 8181179]

Stary HC, Chandler AB, Dinsmore RE, Fuster V, Glagov S, Insull W, Rosenfeld ME, Schwartz CJ, Wagner WD, Wissler RW. A Definition of advanced types of atherosclerotic lesions and the histological classification of atherosclerosis. A report from the Committee on Vascular Lesions of the Council on Arteriosclerosis, AHA. Circulation. 1995; 92:1355–1374. [PubMed: 7648691]

Steinman DA. Image-based computational fluid dynamics modeling in realistic arterial geometries. Ann Biomed Eng. 2002; 30(4):483–497. [PubMed: 12086000]

Stone GW, Mintz GS. Letter by Stone and Mintz regarding article, unreliable assessment of necrotic core by virtual histology intravascular ultrasound in porcine coronary artery disease. Circ Cardiovasc Imaging. 2010; 3(5):e4. [PubMed: 20841552]

Stone PH, Saito S, Takahashi S, Makita Y, Nakamura S, Kawasaki T, Takahashi A, Katsuki T, Nakamura S, Namiki A, Hirohata A, Matsumura T, Yamazaki S, Yokoi H, Tanaka S, Otsuji S, Yoshimachi F, Honye J, Harwood D, Reitman M, Coskun AU, Papafaklis MI, Feldman CL. PREDICTION Investigators. Prediction of progression of coronary artery disease and clinical outcomes using vascular profiling of endothelial shear stress and arterial plaque characteristics: the PREDICTION Study. Circulation. 2012; 126(2):172–181. [PubMed: 22723305]

Tang, D. Modeling flow in healthy and stenosed arteries. In: Hoboekn, Metin Akay, editor. Wiley Encyclopedia of Biomedical Engineering. John Wiley & Sons, Inc; New Jersey: 2006. Article 1525

Tang D, Teng ZZ, Canton G, Hatsukami TS, Dong L, Huang X, Yuan C. Local critical stress correlates better than global maximum stress with plaque morphological features linked to atherosclerotic plaque vulnerability: an in vivo multi-patient study. Biomed Eng Online. 2009a; 8:15. http://dx.doi.org/10.1186/1475-925X-8-15. [PubMed: 19650901]

Tang D, Teng Z, Canton G, Yang C, Ferguson M, Huang X, Zheng J, Woodard PK, Yuan C. Sites of rupture in human atherosclerotic carotid plaques are associated with high structural stresses: an in vivo MRI-based 3D fluid-structure interaction study. Stroke. 2009b; 40(10):3258–3263. Featured article on MDlinx.com. [PubMed: 19628799]

Tang D, Yang C, Kobayashi S, Zheng J, Woodard PK, Teng Z, Billiar K, Bach R, Ku DN. 3D MRI-based anisotropic FSI models with cyclic bending for human coronary atherosclerotic plaque mechanical analysis. J Biomech Eng. 2009c; 131(6):061010. [PubMed: 19449964]

Tang D, Yang C, Mondal S, Liu F, Canton G, Hatsukami TS, Yuan C. A negative correlation between human carotid atherosclerotic plaque progression and plaque wall stress: in vivo MRI-based 2D/3D FSI models. J Biomech. 2008; 41(4):727–736. [PubMed: 18191138]

Tang D, Yang C, Zheng J, Woodard PK, Saffitz JE, Petruccelli JD, Sicard GA, Yuan C. Local maximal stress hypothesis and computational plaque vulnerability index for atherosclerotic plaque assessment. Ann Biomed Eng. 2005; 33(12):1789–1801. [PubMed: 16389527]

Tang D, Yang C, Zheng J, Woodard PK, Sicard GA, Saffitz JE, Yuan C. 3D MRI-based multi-component FSI models for atherosclerotic plaques, a 3-D FSI model. Ann Biomed Eng. 2004; 32(7):947–960. [PubMed: 15298432]

Tearney GJ, Regar E, Akasaka T, Adriaenssens T, Barlis P, Bezerra HG, Bouma B, Bruining N, Cho JM, Chowdhary S, Costa MA, de Silva R, Dijkstra J, Di Mario C, Dudek D, Falk E, Feldman MD, Fitzgerald P, Garcia-Garcia HM, Gonzalo N, Granada JF, Guagliumi G, Holm NR, Honda Y, Ikeno F, Kawasaki M, Kochman J, Koltowski L, Kubo T, Kume T, Kyono H, Lam CC, Lamouche G, Lee DP, Leon MB, Maehara A, Manfrini O, Mintz GS, Mizuno K, Morel MA, Nadkarni S, Okura H, Otake H, Pietrasik A, Prati F, Räber L, Radu MD, Rieber J, Riga M, Rollins A, Rosenberg M, Sirbu V, Serruys PW, Shimada K, Shinke T, Shite J, Siegel E, Sonoda S, Suter M, Takarada S, Tanaka A, Terashima M, Thim T, Uemura S, Ughi GJ, van Beusekom HM, van der Steen AF, van Es GA, van Soest G, Virmani R, Waxman S, Weissman NJ, Weisz G. International Working Group for Intravascular Optical Coherence Tomography (IWG-IVOCT). Consensus standards for acquisition, measurement, and reporting of intravascular optical coherence tomography studies: a report from the International Working Group for Intravascular Optical

Coherence Tomography Standardization and Validation. J Am Coll Cardiol. 2012; 59(12):1058–1072. [PubMed: 22421299]

Teng Z, Canton G, Yuan C, Ferguson M, Yang C, Huang X, Zheng J, Woodard PK, Tang D. 3D critical plaque wall stress is a better predictor of carotid plaque rupture sites than flow shear stress: an in vivo MRI-based 3D FSI study. J Biomech Eng. 2010; 132(3):031007. [PubMed: 20459195]

Thim T, Hagensen MK, Wallace-Bradley D, Granada JF, Kaluza GL, Drouet L, Paaske WP, Bøtker HE, Falk E. Unreliable assessment of necrotic core by virtual histology intravascular ultrasound in porcine coronary artery disease. Circ Cardiovasc Imaging. 2010; 3(4):384–391. [PubMed: 20460496]

Underhill HR, Hatsukami TS, Fayad ZA, Fuster V, Yuan C. MRI of carotid atherosclerosis: clinical implications and future directions. Nat Rev Cardiol. 2010; 7(3):165–173. [PubMed: 20101259]

Vengrenyuk Y, Cardoso L, Weinbaum S. Micro-CT based analysis of a new paradigm for vulnerable plaque rupture: cellular microcalcifications in fibrous caps. Mol Cell Biomech. 2008; 5(1):37–47. [PubMed: 18524245]

Vengrenyuk Y, Carlier S, Xanthos S, Cardoso L, Ganatos P, Virmani R, Einav S, Gilchrist L, Weinbaum S. A hypothesis for vulnerable plaque rupture due to stress-induced debonding around cellular microcalcifications in thin fibrous caps. Proc Natl Acad Sci USA. 2006; 103(40):14678–14683. [PubMed: 17003118]

Virmani R, Kolodgie FD, Burke AP, Farb A, Schwartz SM. Lessons from sudden coronary death: a comprehensive morphological classification scheme for atherosclerotic lesions. Arterioscler Thromb Vasc Biol. 2000; 20(5):1262–1275. [PubMed: 10807742]

Virmani R, Ladich ER, Burke AP, Kolodgie FD. Histopathology of carotid atherosclerotic disease. Neurosurgery. 2006; 59:S219–S227. [PubMed: 17053606]

Wentzel JJ, Corti R, Fayad ZA, Wisdom P, Macaluso F, Winkelman MO, Fuster V, Badimon JJ. Does shear stress modulate both plaque progression and regression in the thoracic aorta? Human study using serial magnetic resonance imaging. J Am Coll Cardiol. 2005; 45(6):846–854. [PubMed: 15766817]

Williamson SD, Lam Y, Younis HF, Huang H, Patel S, Kaazempur-Mofrad MR, Kamm RD. On the sensitivity of wall stresses in diseased arteries to variable material properties. J Biomech Eng. 2003; 125:147–155. [PubMed: 12661209]

Wu Z, Yang C, Tang D. In vivo serial MRI-based models and statistical methods to quantify sensitivity and specificity of mechanical predictors for carotid plaque rupture: location and beyond. J Biomech Eng. 2011; 133(6):064503. [PubMed: 21744932]

Yang C, Bach R, Zheng J, El Naqa I, Woodard PK, Teng ZZ, Billiar KL, Tang D. In vivo IVUS-based 3D fluid structure interaction models with cyclic bending and anisotropic vessel properties for human atherosclerotic coronary plaque mechanical analysis. IEEE Trans Biomed Eng. 2009; 56(10):2420–2428. [PubMed: 19567341]

Yang C, Canton G, Yuan C, Ferguson M, Hatsukami TS, Tang D. Advanced human carotid plaque progression correlates positively with flow shear stress: an in vivo MRI multi-patient 3D FSI study. J Biomech. 2010; 43(13):2530–2538. [PubMed: 20570268]

Yang C, Tang D, Yuan C, Hatsukami TS, Zheng J, Woodard PK. In vivo/ex vivo MRI-based 3D models with fluid–structure interactions for human atherosclerotic plaques compared with fluid/wall-only models. CMES: Comput Model Eng Sci. 2007; 19(3):233–245.

Yuan C, Mitsumori LM, Beach KW, Maravilla KR. Special review: carotid atherosclerotic plaque: noninvasive MR characterization and identification of vulnerable lesions. Radiology. 2001a; 221:285–299. [PubMed: 11687667]

Yuan C, Mitsumori LM, Ferguson MS, Polissar NL, Echelard DE, Ortiz G, Small R, Davies JW, Kerwin WS, Hatsukami TS. In vivo accuracy of multispectral MR imaging for identifying lipid-rich necrotic cores and intra-plaque hemorrhage in advanced human carotid plaques. Circulation. 2001b; 104:2051–2056. [PubMed: 11673345]

Zhang Y, Bajaj C, Sohn BS. 3D finite element meshing from imaging data. Comput Methods Appl Mech Eng. 2005; 194(48–49):5083–5106. [PubMed: 19777144]

Zhang Y, Hughes TJ, Bajaj CL. An automatic 3D mesh generation method for domains with multiple materials. Comput Methods Appl Mech Eng. 2010; 199(5–8):405–415. [PubMed: 20161555]

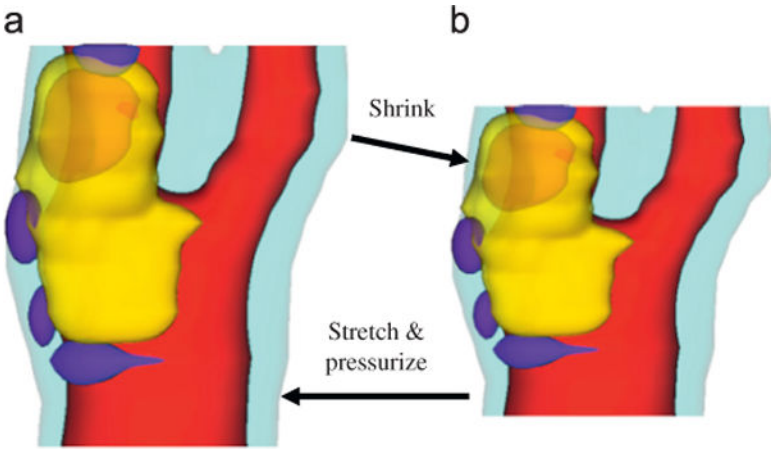

Fig. 1.

Illustration of the shrink–stretch process. The total plaque volume should be conserved. Yellow: lipid; blue: calcification; light blue: outer wall; red: lumen. (a) In vivo shape and (b) numerical start shape. (For interpretation of the references to color in this figure legend, the reader is referred to the web version of this article.)

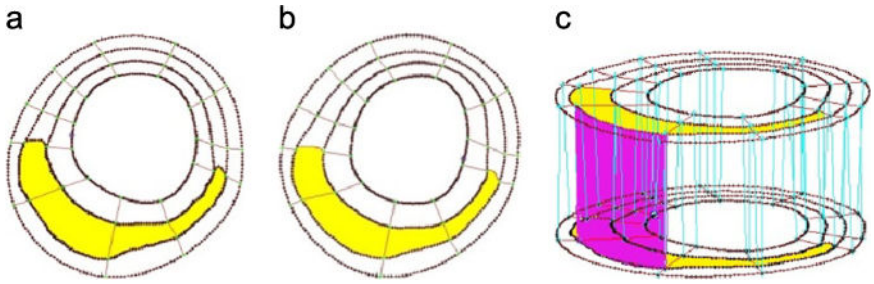

Fig. 2.

The component-fitting mesh generation process. (a) and (b) Two slices (A and B) with a lipid core inclusion (yellow) and numerically-generated component-fitting curves and surfaces; (c) component-fitting volumes formed by connecting corresponding areas from adjacent slices. (For interpretation of the references to color in this figure legend, the reader is referred to the web version of this article.)

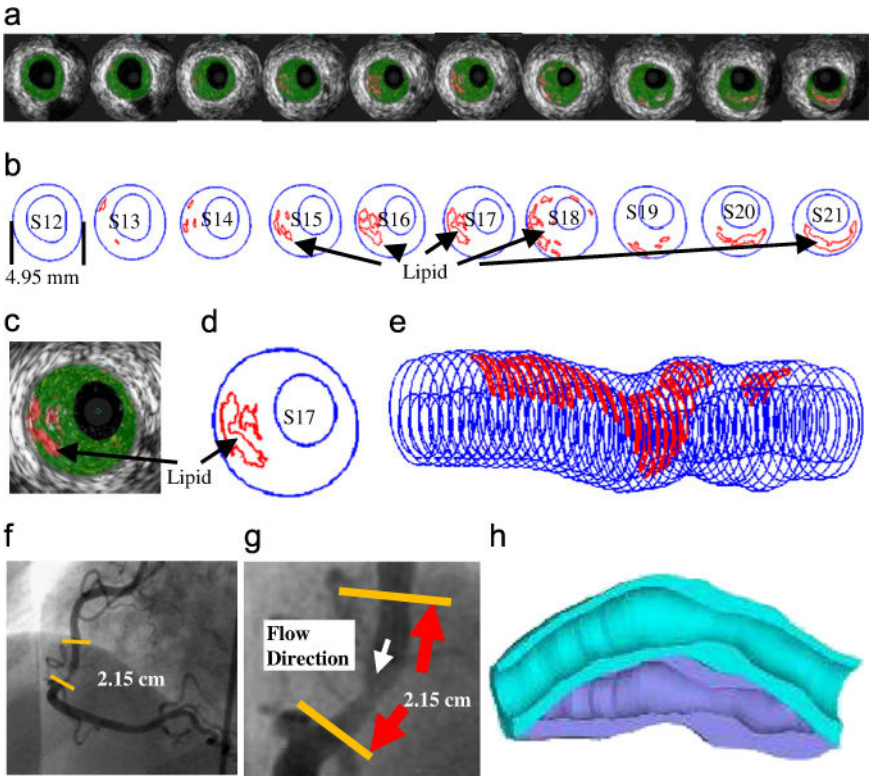

Fig. 3.

IVUS model construction process: (a) selected 10 slices from a 44-slice IVUS data set with IVUS-VH; (b) contour plots; (c) enlarged view; (d) enlarged contour plot; (e) 3D plaque geometry showing lipid core locations; (f) angiography showing location of the lesion and vessel curvature; (g) enlarged angiography showing the lesion; (h) illustration of vessel bending.

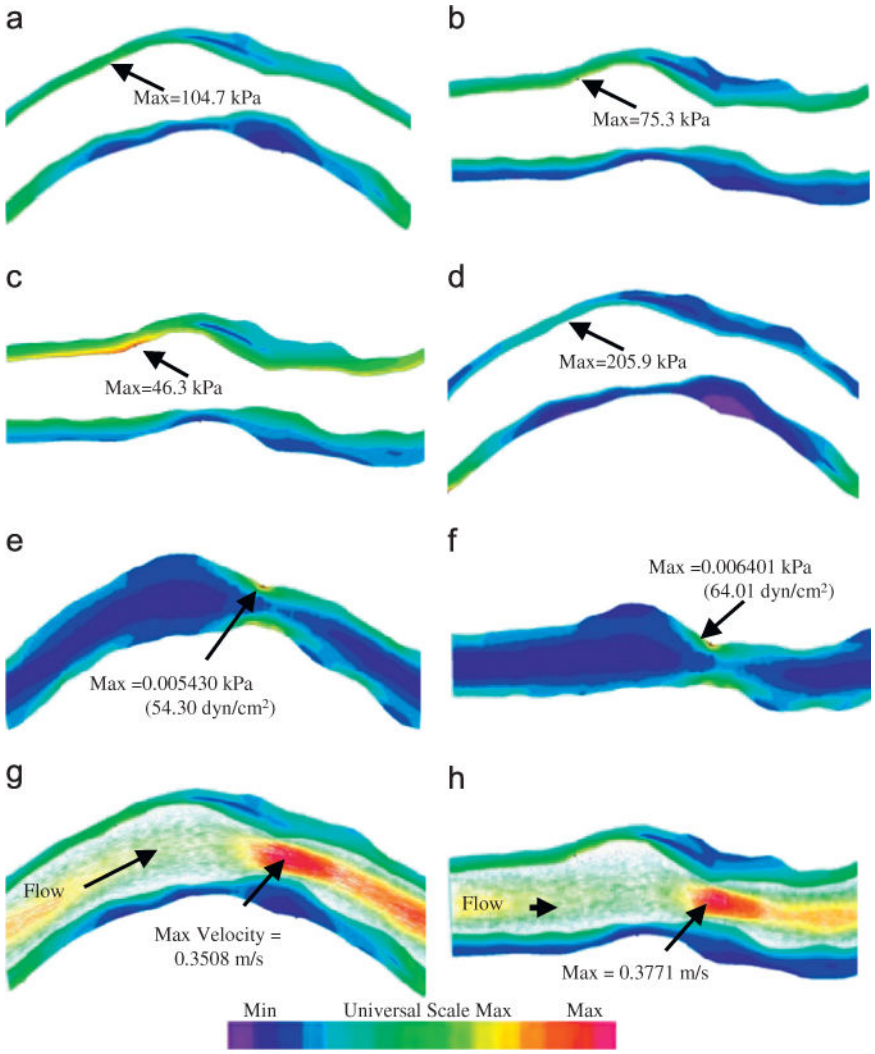

Fig. 4.

Plaque wall stress, flow shear stress and velocity plots from four models showing vessel bending, anisotropic vessel properties and axial stretch have considerable effect on stress/strain distributions and modest impact on flow features. κ is the curvature of the displacement curve imposed at the lower edge of the vessel (side of myocardium). Pin: pressure condition imposed at the inlet of the vessel. (a) M1, Pin=86 mmHg, curvature κ=97 m^{-1}, (b) M2, Pin=86 mmHg, no bending, (c) M3, Pin=86 mmHg, no bending, (d) M4, Pin=86 mmHg, κ=97 m^{-1}, (e) M1, FMSS, Pin=86 mmHg, κ=97 m^{-1}, (f) M2, FMSS, Pin=86mmHg, no bending, (g) M1, velocity, Pin=86 mmHg, κ=97 m^{-1} and (h) M2, velocity, Pin=86 mmHg, no bending

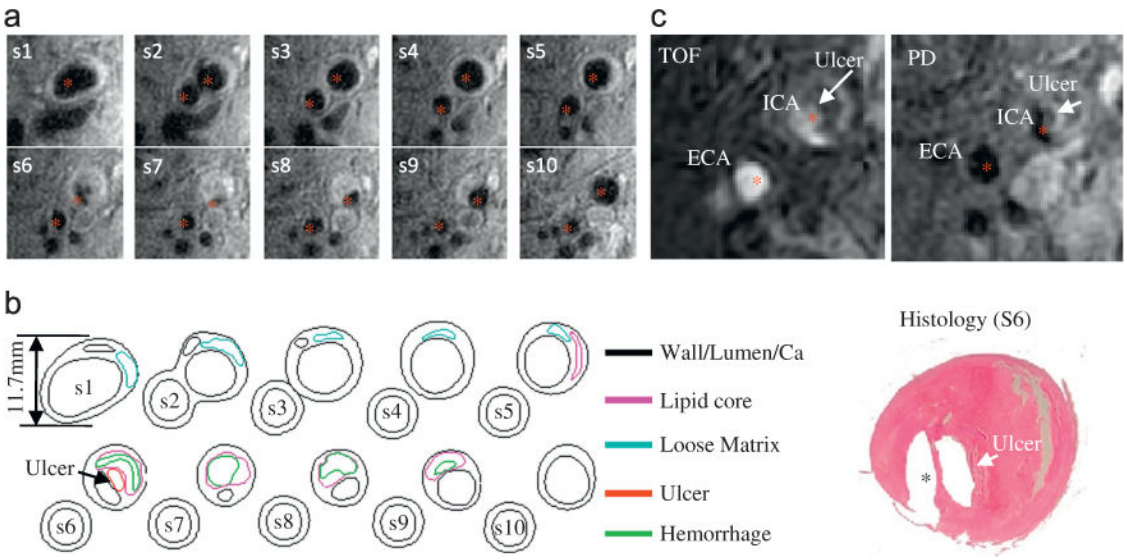

Fig. 5.

A sample human carotid plaque showing ulceration. (a) T1-weighted in vivo MR-images of a Human Carotid Plaque, (b) corresponding Segmented Contour Plots with components and (c) presence of ulceration validated by histology.

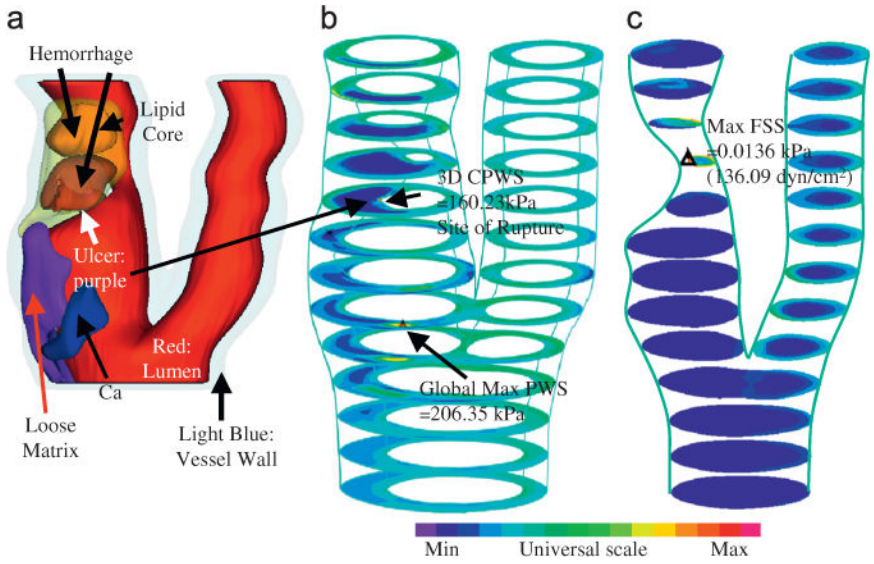

Fig. 6.

Modeling results from one plaque sample showing CPWS was able to predict the actual rupture site while CFSS failed to do so. (a) 3D rendered transparent view, (b) stress-P_1, stack view and (c) FSS, stack view.

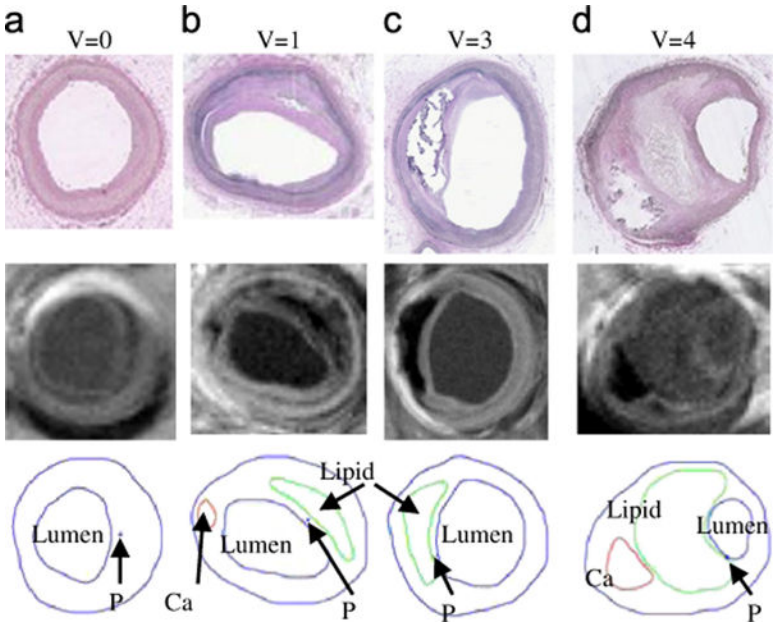

Fig. 7.

Selected plaque samples with different vulnerability classified by histopathological analysis (Tang et al., 2005). (a) Very Stable ***V***=0, (b) stable plaque ***V***=1, (c) unstable ***V***=3 and (d) very unstable ***V***=4.

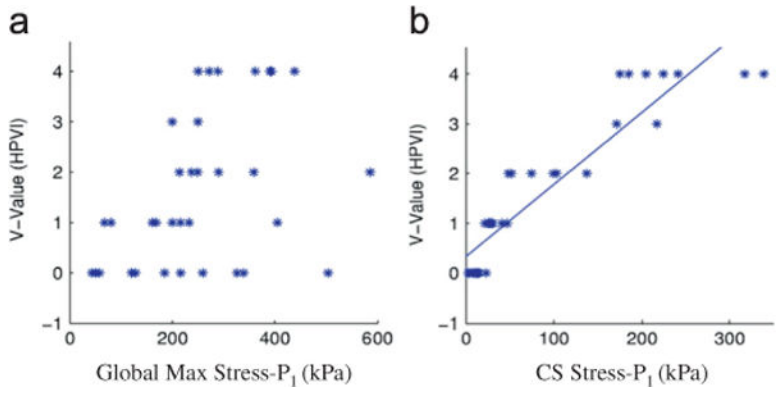

Fig. 8.

Critical plaque wall stress shows much better correlation with HPVI than global maximum plaque wall stress from 34 coronary 2D plaque samples. P<0.0001 (Tang et al., 2005). (a) HPVI vs. global max stress-P_1 and (b) HPVI vs. critical stress.

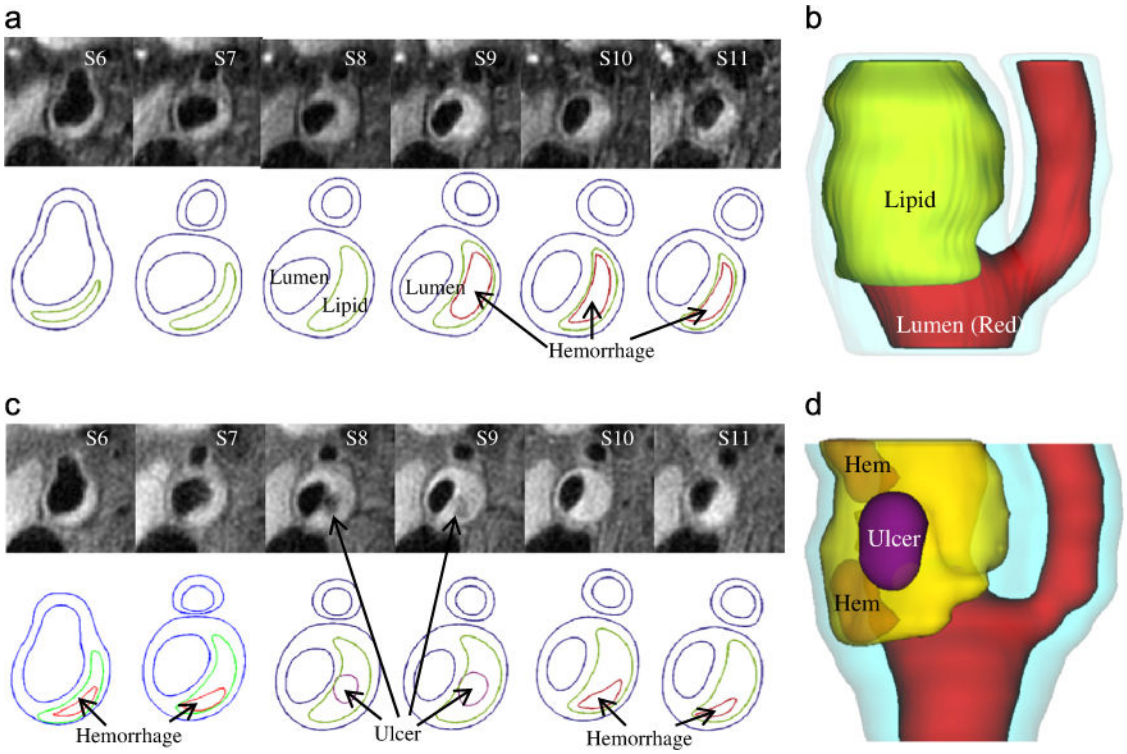

Fig. 9.

In vivo MR images (T1 weighting) of a human carotid plaque at baseline (Time 1) and follow-up (Time 2) with ulceration observed at Time 2. Transparent view was used to show location of ulcer. Color in 3D plot: red: lumen; light blue: outside vessel wall; yellow: lipid; purple: ulcer; orange: hemorrhage. (a) MRI and contours at time 1 showing lipid core, (b) 3D view of the plaque at T1, (c) MRI and contours at time 2 showing ulcer and (d) 3D view at T2 showing ulcer and hemorrhage. (For interpretation of the references to color in this figure legend, the reader is referred to the web version of this article.)

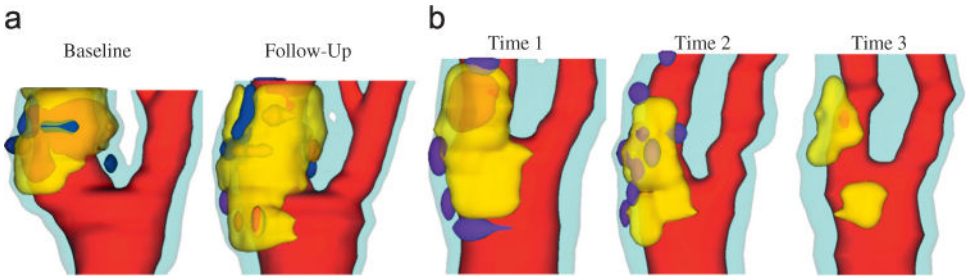

Fig. 10.

3D human carotid plaque samples re-constructed from in vivo MR images showing progression and regression. Time interval: 18 months. Red: lumen; yellow: lipid; dark blue: calcification; light blue: outer wall. (a) Plaque showing progression and (b) plaque showing regression. (For interpretation of the references to color in this figure legend, the reader is referred to the web version of this article.)

Table 1

Comparison of 3D critical plaque wall stress (CPWS) and critical flow shear stress (CFSS) between Group 1 and Group 2 (1 kPa=10^4 dyn/cm^2).

3D CPWS (kPa)				**3D CFSS (dyn/cm^2)**			
Group 1		**Group 2**		**Group 1**		**Group 2**	
P1	457.85	P7	127.59	P1	112.47	P7	78.99
P2	241.90	P8	86.68	P2	96.13	P8	41.59
P3	193.31	P9	129.31	P3	86.27	P9	77.57
P4	160.23	P10	165.06	P4	136.09	P10	38.89
P5	348.19	P11	103.68	P5	70.00	P11	34.30
P6	179.14	P12	151.90	P6	56.70	P12	34.55
		P13	143.70			P13	32.65
		P14	114.52			P14	31.90
		P15	110.38			P15	129.22
		P16	108.03			P16	26.78
		P17	104.57			P17	59.73
		P18	247.86			P18	46.21
Mean ± SD	263.44 ± 116.72	Mean ± SD	132.77 ± 42.67	Mean ± SD	92.94 ± 28.77	Mean ± SD	52.70 ± 29.76

Table 2

Morphological plaque vulnerability index (MPVI) definition and AHA classifications.

MPVI	Plaque	Description	AHA classification
V=0	Very stable	Normal or slight intimal thickening	Type I, some atherogenic lipoprotein and intimal thickening
V=1	Stable	Moderate intimal thickening, no extracellular lipid, calcification or significant inflammation	Type II (fatty streak), III (preatheroma)
V=2	Slightly unstable	Small lipid core (<30% of plaque size); calcification may be present; thick fibrous cap (> 200 μm); little or no inflammation at plaque shoulders	Types IV, Vb, and Vc with less than 30% NC by area; or VII/VIII
V=3	Moderately unstable	Moderate lipid core (30–40% of plaque size) and fibrous cap (150–200 μm); moderate intraplaque hemorrhage; moderate inflammation	Types Va, IV/V with 30–40% NC by area
V=4	Highly unstable	Large lipid core(440%); thin fibrous cap (<150 μm); large intraplaque hemorrhage; extensive inflammation; evidence of previous plaque rupture	Types VI; IV/V with > 40% NC by area

Table 3

Stress-based plaque classification may be able to differentiate advanced vulnerable plaques (AHA Types V, VI, VII plaques) (152 in vivo slices).

CPVI score	0	1	2	3	4
AHA Type V (99 cases)	4	32	26	17	20
AHA Type VI (32 cases)	2	3	7	6	14
AHA VII (21 cases)	9	7	1	1	3

Table 4

The accuracy of the best Generalized Linear Mixed-Effects Models (GLMM) for predicting ulcer nodes (600 points). Sensitivity of prediction is defined as the proportion of the true positive-outcomes that are predicted to be positive. Specificity of prediction is defined as the proportion of the true negative-outcomes that are correctly predicted to be negative (Garrett et al., 2004).

Probability threshold	PWS (plaque wall stress)			PWSn (plaque wall strain)			FSS (flow shear stress)		
	Sensitivity	Specificity	Sum	Sensitivity	Specificity	Sum	Sensitivity	Specificity	Sum
0.5	0.727	0.982	**1.709**	0.485	0.984	**1.469**	0.273	0.986	**1.259**
0.3	0.788	0.968	**1.756**	0.515	0.968	**1.483**	0.758	0.928	**1.686**
0.2	0.818	0.958	**1.776**	0.606	0.963	**1.569**	0.939	0.903	**1.842**
	PWS + FSS			PWSn + FSS			PWS + PWSn		
0.5	0.909	0.94	**1.849**	0.939	0.928	**1.867**	0.909	0.977	**1.886**
0.3	0.939	0.933	**1.872**	0.939	0.921	**1.86**	**0.97**	**0.958**	**1.928**
0.2	0.939	0.928	**1.867**	0.939	0.908	**1.847**	0.97	0.944	**1.914**
				PWS + PWSn+ FSS					
0.5				0.939	0.905	**1.844**			
0.3				0.939	0.903	**1.842**			
0.2				0.939	0.898	**1.837**			